Inorganic Chemistry
Article

Inorg. Chem. **2009**, *48*, 8751–8758 **8751**
DOI: 10.1021/ic900805g

Crystallography of Chevrel Phases, MMo_6T_8 (M = Cd, Na, Mn, and Zn, T = S, Se) and Their Cation Mobility

E. Levi,*,† G. Gershinsky,† D. Aurbach,† and O. Isnard‡,§

†*Department of Chemistry, Bar-Ilan University, Ramat-Gan, Israel 52900,* ‡*Institut Néel, CNRS & Université de Grenoble J. Fourier, BP166X, 38042 Grenoble cédex 9, France, and* §*Institut Laue Langevin, BP 156 X, 38042 Grenoble cédex 9, France*

Received April 26, 2009

Chevrel phases (CPs), $M_xMo_6T_8$ (M = metal, T = S, Se) are unique materials, which allow for a fast and reversible insertion of various cations at room temperature. In spite of extensive studies of these materials, the origin of their high ionic mobility remained unclear. In a previous paper we presented for the first time a proper classification of the very complex transport behavior of different cations in the Mo_6T_8 hosts: (i) apparent immobility of the large M cations such as Pb^{2+}, Sn^{2+}, Ag^+ in the ternary phases, MMo_6T_8; (ii) coupled M+M′ diffusion in the quaternary phases, $M_xM'_yMo_6T_8$, where both large and small cations can assist; (iii) cation trapping in the Mg−Mo_6S_8, Cd−Mo_6S_8, and Na−Mo_6T_8 systems; (iv) a combination of low- and high-rate diffusion kinetics at the first and last intercalation stages, respectively, for the Cu−Mo_6S_8, Mn−Mo_6S_8, and Cd−Mo_6Se_8 systems, and (v) a fast ionic transport for small cations such as Ni^{2+}, Zn^{2+}, and Li^+. It was shown that this behavior could be understood by a relatively simple crystallographic analysis (mapping of all the cation sites and estimations of their potential energy according to the distances of these sites from adjacent anions and cations) of the diffusion routes, which differ for different cations. For this analysis, it was necessary to complete our knowledge about the cation location in the crystal structure for several CPs with known ionic mobility. This article presents the results of a combined Rietveld analysis of powder X-ray and high-resolution neutron diffraction profiles for $NaMo_6T_8$, $ZnMo_6T_8$, $CdMo_6T_8$, and $MnMo_6S_8$. All seven compounds can be defined as classic CPs, where cation delocalization from the center of the largest cavity between the Mo_6T_8 blocks decreases with the length of the ideal chemical bond, M−T. In addition, this work details the effect of the structural parameters on the ionic conductivity in CPs, namely, it shows how subtle changes in cation delocalization may be crucial for diffusion kinetics.

Introduction

The remarkable ionic conductivity of Chevrel phases (CPs), $M_xMo_6T_8$ (M = metal, T = S, Se,Te) remains in the shadow of their striking superconductivity. However, CPs are, at present, the only materials that allow fast and reversible insertion of various cations, monovalent (Li^+, Na^+, Cu^+) as well as divalent Zn^{2+}, Cd^{2+}, Ni^{2+}, Mn^{2+}, Co^{2+}, Fe^{2+}, and Mg^{2+} at ambient temperatures.[1−15] Moreover, the insertion of an M cation into metal-containing CPs, $M'_xMo_6T_8$ ($x \neq 0$), may result in the displacement reaction associated with an unusual coupled M + M′ cation motion in the same crystal structure.[16,17] The key question here is what is so special in CPs that ensures the exceptionally high mobility of multivalent cations?

*To whom correspondence should be addressed. E-mail: elenal@mail.biu.ac.il.

(1) Schollhorn, R.; Kumpers. M.; Besenhard, J. O. *Mater. Res. Bull.* **1977**, *12*, 781.
(2) Schollhorn, R. *Angew. Chem., Int. Ed. Engl.* **1980**, *19*, 983.
(3) Schollhorn, R. In *Inclusion Compounds*, Vol. *1*; Atwood, J. L. Ed.; Academic Press: London, 1984.
(4) Tarascon, J. M.; Hull, G. W.; Marsh, P.; Ter Haar. *J. Solid State Chem.* **1987**, *66*, 204.
(5) Gocke, E.; Schramm, W.; Dolscheid, P.; Schollhorn, R. *J. Solid State Chem.* **1987**, *70*, 71.
(6) Gocke, E.; Schollhorn, R.; Aselmann, G.; Muller-Warmuth, W. *Inorg. Chem.* **1987**, *26*, 1805.
(7) Weppner, W.; Huggins, R. A. *Annu. Rev. Mater. Sci.* **1978**, *8*, 269.
(8) Boulanger, C.; Lecuire, J.-M. *Electrochem. Acta* **1987**, *32*, 345.
(9) Boulanger, C.; Lecuire, J.-M. *Electrochem. Acta* **1988**, *33*, 1561; 1567; 1573.
(10) Janssen, M.; Eckert, H.; Muller-Warmuth, W.; Stege, U.; Schollhorn, R. *Chem. Mater.* **1998**, *10*, 3459.
(11) Ritter, C.; Gocke, E.; Fischer, C.; Schollhorn, R. *J. Mater. Res. Bull.* **1992**, *27*, 1217.
(12) Ritter, C.; Noldeke, C.; Press, W.; Stege, U.; Schollhorn, R. *Z. Phys. B* **1993**, *92*, 437.
(13) Fischer, C.; Gocke, E.; Stege, U.; Schollhorn, R, *J. Solid State Chem.* **1993**, *102*, 54.
(14) Aurbach, D.; Lu, Z.; Schechter, A.; Gofer, Y.; Gizbar, H.; Turgeman, R.; Cohen, Y.; Moskovich, M.; Levi, E. *Nature* **2000**, *407*, 724.
(15) Seghir, S.; Boulanger, C.; Diliberto, S.; Lecuire, J.-M.; Potel, M.; Merdrignac-Conanec, O. *Electrochem. Commun.* **2008**, *10*, 1505.
(16) Levi, E.; Mitelman, A.; Aurbach, D.; Brunelli, M. *Chem. Mater.* **2007**, *19*, 5131 (and references therein).
(17) Mitelman, A.; Levi, M. D.; Lancry, E.; Levi, E.; Aurbach, D. *Chem. Commun.* **2007**, 4212.

Published on Web 08/25/2009

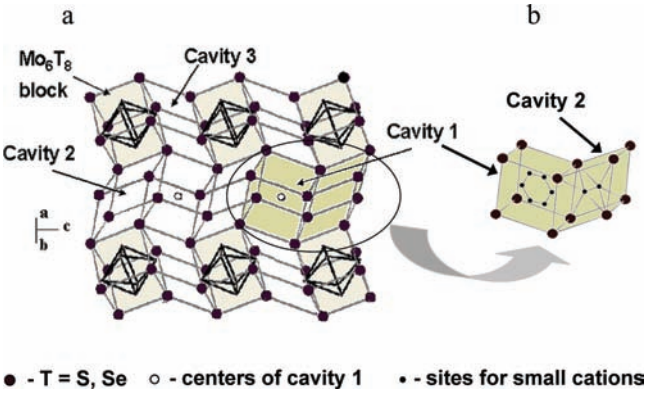

Figure 1. (a) Basic CPs' crystal structure: three types of cavities between Mo_6T_8 blocks and the diffusion channel in direction c (one of three equivalent directions in rhombohedral crystals) formed by face-sharing pseudo-cubes of cavities 1 and 2. (b) The site arrangements in cavities 1 and 2: case of small cations.

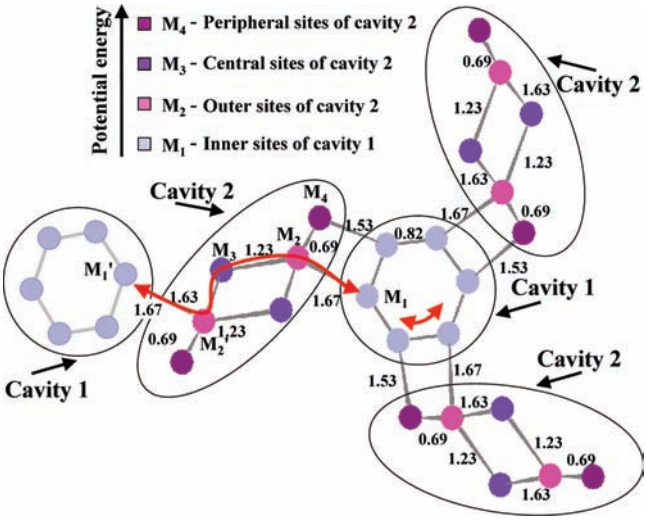

Figure 2. Simplified typical map of all the cation sites in CPs and two competing diffusion pathways of inserted ions (marked in red).

At first glance, CPs can be characterized as typical intercalation compounds with an open three-dimensional channel system, formed by face-sharing pseudo-cubic cavities between Mo_6T_8 blocks, although the latter are really unusual. In contrast to common ionic compounds where each cation is surrounded by anions, in CPs six Mo cations or a whole octahedral cluster is coordinated by an ion cube.[18,19] In earlier work,[3,5] the high cation diffusivity in CPs was ascribed to the hypothetical quasi-monovalent state of the inserting cations as transients, which results from a rapid one-electron transfer via the Mo_6T_8 matrix, for example, $Zn^{2+} + e- \leftrightarrow Zn^{+}$. Alternatively, we explained the exceptional ionic conductivity in CPs by a fast and efficient attainment of local electroneutrality by the Mo_6-cluster, which is capable of taking up easily up to 4 electrons.[20] However, it remained unclear why the Mo_6-cluster ensures high mobility for some cations at room temperature (RT), while for others (about 30 additional cations) the insertion happens only at elevated temperatures.

According to common knowledge,[3−5] the main parameter that determines the cation mobility in CPs is its size: large cations (radius > 1 Å) located in the origin of pseudo-cubic cavity 1 (Figure 1a, cation coordination number, CN = 8 or 2) fall into a combined energetic/steric trap and inhibit any ionic transport. In contrast, small cations (radius < 1 Å), shifted ("delocalized") from the origin and randomly distributed between 12 tetrahedral sites (so-called inner and outer rings) in cavities 1 and 2 (Figure 1b) are highly mobile. In the separate, theoretical part of this work,[21] we revised the available experimental data concerning the ionic mobility in CPs. It was shown that the transport behavior in CPs cannot be understood within the framework of the blocking concept; it is much more complex and includes the following: (i) apparent immobility of large M cations, like Pb^{2+}, Sn^{2+}, and Ag^{+} in the ternary phases, MMo_6T_8; (ii) coupled M + M′ diffusion in the quaternary phases, $M_xM'_yMo_6T_8$ (M and M′ = small or large cations); (iii) cation trapping in the Mg−Mo_6S_8, Cd−Mo_6S_8, and Na−Mo_6T_8 systems; (iv) a combination of low and high rate diffusion kinetics at the first and last intercalation stages, respectively, for the Cu−Mo_6S_8, Mn−Mo_6S_8, and Cd−Mo_6Se_8 systems; and (v) a fast ionic transport for small cations such as Ni^{2+}, Zn^{2+}, and Li^{+}.

To explain all the peculiarities of ionic transport in CPs, we analyzed the diffusion routes of different cations in the CPs' crystal structure.[21] Our analysis was based on the mapping of all the cation sites, including the transient transport ones (Figure 2), as well as on the estimation of their potential energy according to the distances of these sites from adjacent anions and cations. As a result, we demonstrated two competing diffusion pathways for most of the CPs: circular motion within cavity 1 with activation energy E_c (between M_1 sites of the inner ring), and progressive diffusion from one cavity 1 (or 2) to the neighboring one, with activation energy E_d (commonly, the $M_1-M_2-M_3-M_2'-M_1'$ pathway). It was shown that the character of the ionic transport depends mostly on the distribution of the repulsive forces between the inserted cations, as well as on the E_d/E_c ratio, affected in turn by the cation position, its size, cation-Mo interactions, and the anion nature.

Such diffusion analysis requires knowledge of the exact crystal structures for the intercalation compounds. In the previous part of this study[21] it was shown that the kinetic problems in CPs exist only at the first stage of cation insertion (commonly for $0 < x < 1$), while the compounds with higher intercalation levels always show fast ion transport because of cation−cation repulsion. Thus, to explain the kinetic problems, we have to focus on the $M_xMo_6T_8$ compounds with stoichiometry $x = 1$. Accordingly, we used the available literature data, and also performed X-ray and neutron refinements for a number of unknown crystal structures. This article presents the experimental part of the study, namely, the structural determinations for several M-Mo_6T_8 systems with known ionic conductivity. In addition, the aim of this paper is to illustrate in detail the effect of the structural parameters on the ionic transport in CPs.

(18) Yvon, K. In *Current Topics in Material Science*; Vol. *3*; Kaldis, E., Ed.; Elsevier: North-Holland, Amsterdam, 1979.
(19) *Topics in Current Physics: Superconductivity in Ternary Compounds I*; Fisher. Q., Maple. M. B., Eds.; Springer-Verlag: Berlin, 1982.
(20) Levi, E.; Levi, M. D.; Chasid, O.; Aurbach, D. *J. Electroceram.* **2009**, *22*,13.
(21) Levi, E.; Gershinsky, G.; Aurbach, D.; Isnard, O.; Ceder, G. *Chem. Mater.* **2009**, *21*, 1390.

Table 1. Samples' Characterization (the Results of the Rietveld Refinement of the Diffraction Profiles)

				lattice parameters			additional		fitting quality		
N	phase under study	synthesis	diffraction	a_h(Å)	c_h(Å)	a_r(Å)	α(°)	phases	impurities	Chi2	R_B,%	R_F,%
1	$NaMo_6S_8$	chem. interc. from benzophenone/THF solution	X-ray	9.226	11.228	6.510	90.24	29%Na_2MoO_4*2H_2O	<2% Mo_2C	1.20	1.30	1.11
2		chem. interc. from liquid NH_3	neutron	9.231	11.237	6.514	90.23	13%Mo_6S_8	4%Na_2MoO_4		5.09	2.89
3	$NaMo_6Se_8$	chem. interc. from benzophenone/THF solution	X-ray	9.572	11.716	6.767	90.02	16% Mo_6Se_8	14% $MoSe_2$ 8% Na_2MoO_4	1.58	4.65	4.16
4	$CdMo_6Se_8$	thermal interc. at 450 °C, 36 h	X-ray	9.415	10.737	6.508	92.66	8%MoO_2	1% CdS 1% MoS_2	0.86	3.71	2.90
5			neutron	9.424	10.750	6.515	92.65		4% MoO_2 0.5% MoC		1.96	1.03
6	$CdMo_6Se_8$		X-ray	9.782	11.181	6.767	92.58		2% $MoSe_2$	1.13	5.05	3.39
7			neutron	9.793	11.192	6.774	93.50		2% $MoSe_2$ 0.4% Mo 1% Mo_6Se_8		1.98	1.04
8	$MnMo_6S_8$	synthesis from the elements at 1100 °C, 72 h	X-ray	9.448	10.526	6.486	93.58	16% Mo_2S_3	7% Mo_2% MnS 3% MoS_2	2.54	5.19	1.76
9			neutron	9.467	10.523	6.495	93.58	26% Mo_6S_8	7% MoS_2 1% MoC 1% MoO_2 1% Mn		3.85	2.04
10	$ZnMo_6S_8$		X-ray	9.531	10.286	6.484	94.62		4% Mo_2C ~2% ZnS	1.86	4.22	2.90
11			neutron	9.454	10.296	6.492	94.63	6% Mo_6S_8	4% Mo_2C ~2% ZnS 0.5% MoC		3.71	1.97
12	$ZnMo_6Se_8$		X-ray	9.900	10.719	6.741	94.50	22% Mo_6Se_8	~2% ZnSe 1% Mo 1% MoO2	2.78	6.33	3.42
13			neutron	9.910	10.732	6.748	94.50	29% Mo_6Se_8			2.75	1.66

Experimental Section

CPs can be obtained by thermal, chemical, or electrochemical intercalation. Our choice of synthetic methods was defined mainly by research techniques requirements. For instance, a relatively high sample mass needed for neutron diffraction (~3−5 g), as well as the negative effect of the carbon black and the organic binder (mandatory components of composite electrodes) on the peak-noise ratio in the neutron patterns, excluded the use of electrochemical insertion. In addition, our previous experience[16,23] shows that, for any synthetic method, the intrinsic instability of CPs commonly results in the formation of oxides or products of material deintercalation.

The preparation of the hosts, Mo_6T_8 (T = S, Se), was described earlier.[22,24] The products of the chemical Na insertion, $NaMo_6T_8$, was obtained via the topotactic reaction of the binary Mo_6T_8 in contact with a benzophenone/Na/THF solution (in the inert atmosphere of an Ar glovebox) as the source of Na^+ ions and as the reducing agent:

$$Na + Ph_2CO \rightarrow Na^+Ph_2CO^-$$

MMo_6T_8 (M = Zn, Mn) were synthesized by the reaction of the element powder mixtures in evacuated sealed quartz ampules, which were heated up to 1100 °C for 72 h with dwelling steps at 450 and 700 °C, each for 24 h. The syntheses of $CdMo_6T_8$ were carried out in stainless steel Swagelok cells (assembled in the inert Ar atmosphere) at 450 °C for 36 h and quenched in liquid nitrogen. The starting materials were Cd metal and the host, Mo_6T_8. A good Rietveld fitting for the Cd-containing CPs was obtained when the models included two separate fractions with micro- and nanometric crystallite sizes.

X-ray diffraction (XRD) studies were performed with a Bruker Inc. (Germany) AXS D8 Advance diffractometer (reflection θ-θ geometry; Cu Kα radiation; scintillation counter) with divergence, antiscattering, and receiving slits of 0.3, 0.3, and 0.2 mm, respectively. Diffraction data were collected in the angular range of $10° < 2\theta < 140°$, step size 0.02°, step time 30 s/step.

The neutron diffraction experiments were performed at the Institut Laue Langevin (I.L.L.) at Grenoble, France, on the *D1A* instrument. A detailed description of this instrument is available via the Internet at http://www.ill.fr. *D1A* is a very high resolution powder diffractometer operating with a monochromator takeoff angle of 122°. In the configuration used, the resolution of *D1A* was about 0.3° (fwhm) at 90°. The measurements were carried out at a wavelength of $\lambda = 1.911$ Å, selected by the (115) reflection of a germanium monochromator. During the neutron diffraction measurements, a cylindrical vanadium sample holder of 7 mm inner diameter was used. The neutron detection was performed with a set of 6° spaced ^{3}He counting tubes. The complete diffraction pattern was obtained by scanning over the whole 2θ range.

The data were analyzed by the Rietveld structure refinement program, FULLPROF.[25,26] Thompson−Cox−Hastings pseudo-Voigt functions were used for the peak-shape approximation. The background was refined by a polynomial function (neutron case) or by linear interpolation between background points (X-ray case). The atomic thermal parameters (0.33 Å^2 for Mo, 0.5 Å^2 for S or Se, and 0.5 Å^2 for M

(22) Lancry, E.; Levi, E.; Gofer, Y.; Levi, M.; Salitra, G.; Aurbach, D. *Chem. Mater.* **2004**, *16*, 2832.

(23) Levi, E.; Lancry, E.; Mitelman, A.; Aurbach, D.; Ceder, G.; Morgan, D.; Isnard, O. *Chem. Mater.* **2006**, *18*, 5492.

(24) Levi, E.; Lancry, E.; Mitelman, A.; Aurbach, D.; Isnard O.; Djurado D., *Chem. Mater.* **2006**, *18*, 3705.

(25) Rietveld, H. M. *J. Appl. Crystallogr.* **1969**, *2*, 65.

(26) Carjaval, J. R. *Physica B* **1993**, *192*, 55.

Table 2. Structural Parameters of CPs under Study[a]

		Mo(18f)			T1(18f)			T2(6c)		
N	CP	*x*	*y*	*z*	*x*	*y*	*z*	*x*	*y*	*z*
1	$NaMo_6S_8$	0.0130(3)	0.1744(2)	0.3242(5)	0.3242(5)	0.2901(6)	0.4184(4)	0	0	0.2307(7)
2	$NaMo_6Se_8$	0.0129(5)	0.1696(6)	0.3392(7)	0.3392(7)	0.2980(6)	0.4167(5)		0	0.2288(8)
3	$CdMo_6S_8$	0.0159(2)	0.1727(1)	0.3177(4)	0.3177(4)	0.2830(5)	0.4122(3)	0	0	0.2209(6)
4	$CdMo_6Se_8$	0.0159(3)	0.1668(2)	0.3233(2)	0.3233(2)	0.2870(2)	0.4120(2)	0	0	0.2203(3)
5	$MnMo_6S_8$	0.0148(4)	0.1718(3)	0.3254(7)	0.3254(7)	0.2825(7)	0.4098(6)	0	0	0.2062(9)
6	$ZnMo_6S_8$	0.0165(2)	0.1715(2)	0.3142(4)	0.3142(4)	0.2746(4)	0.4096(3)	0	0	0.2055(6)
7	$ZnMo_6Se_8$	0.0160(2)	0.1649(2)	0.3207(2)	0.3207(2)	0.2816(2)	0.4092(2)	0	0	0.2043(3)

[a] Space group $R\bar{3}$, hexagonal setting, T1 and T2 are anions in general position and on $\bar{3}$ symmetry axis, respectively.

cations) were chosen according to literature data[18] and remained constant. The agreement factors used in this article are defined according to the guidelines of the Rietveld refinement that can be found elsewhere.[27] The neutron scattering lengths used were $b_S = 0.2847\ 10^{-14}$ m, $b_{Se} = 0.7970\ 10^{-14}$ m, $b_{Na} = 0.363\ 10^{-14}$ m, $b_{Zn} = 0.568\ 10^{-14}$ m, $b_{Cd} = 0.487\ 10^{-14}$ m, $b_{Mn} = -0.373\ 10^{-14}$ m, $b_{Mo} = 0.6715\ 10^{-14}$ m, values taken from ref 28. Because of the large neutron absorption cross section of Cd, the Cd-containing samples were measured in a dedicated annular sample holder to maximize the signal over background ratio.

Results and Discussion

Refined Crystal Structures and Maps of Cation Sites. Tables 1 and 2 present the sample characterization and the results of the combined Rietveld analysis performed for the X-ray and neutron diffraction patterns of Na, Zn, Cd, and Mn-containing CPs, namely, their structural parameters and the *R*-factors obtained in the refinement (see also the Rietveld profiles in the Supporting Information). As can be seen, we did not succeed to prepare pure CPs, mostly because of the intrinsic material instability, resulting in the formation of oxides or deintercalated phases. However, the aim of the refinement was reached, as it is evident from the acceptable *R*-factors and the reasonable crystallographic results.

To explain the model used in the fitting, let us recall the basic characteristic features of the CPs' crystal structure. The first of them is the unusually high flexibility of the Mo_6T_8 framework,[31] and its adaptation to cation size and character, which results in respective changes in the energetic structure of these compounds, as well as in a wide variety of structural types.[21,32] In general, according to cation arrangements, all CPs can be divided into two main structural groups, classic and new. In classic CPs,[18,19] the first inserted cation is located in cavity 1, exactly at its origin (type I of classic CPs) or with a shift from the origin (type II of classic CPs). In the latter case, in rhombohedral crystals, the cation occupies randomly one of the six equivalent sites with coordination number (CN) equal to 4 (or 5 for In). This case is shown in Figure 2, where the inner sites have minimal potential energy. Outer sites of cavities 2 with higher potential energy are filled upon subsequent intercalation.

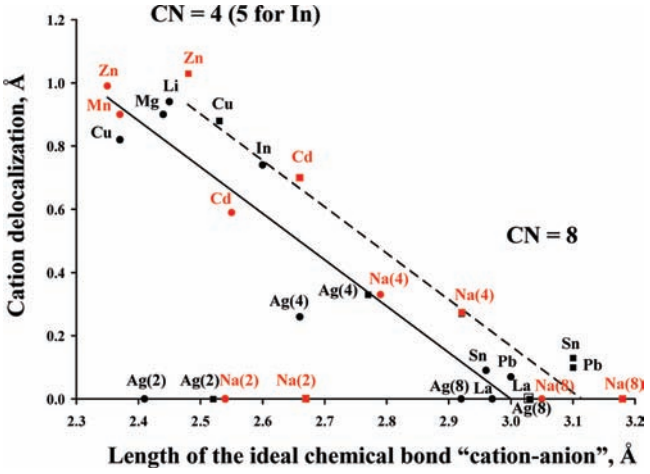

Figure 3. Correlation between the lengths of the ideal chemical bonds "cation-anion" and cations delocalization from the origin of cavity 1. The solid and dashed lines are related to the sulfides and selenides, respectively. The literature data and those obtained in this work are marked in black and red, respectively. The Na and Ag CNs are presented in the parentheses.

In new[29,30] CPs (selenides of transition metals), specific metal−metal interactions between inserted cations and Mo atoms result in the occupation of central sites in cavity 2. More information about factors affecting the cation arrangement in CPs, its correlation to a symmetry of intercalation compounds (rhombohedral or triclinic), as well as polyhedral representations of various structural types, can be found in our previous work.[16,21,23,24,31,32] Note that for all CPs (including fully intercalated compounds), the total number of cation sites greatly exceeds the number of inserted cations. As our study does not include the selenides of transition metals, the classic CP type was chosen as the initial fitting model for all the materials under study.

Another striking peculiarity of CPs is that delocalized and randomly distributed cations may be found not only in the solid solutions, but also in the numerous phases with strict stoichiometry. (Note that a random ion distribution is typically related to non-stoichiometry). In fact, phase diagrams of the systems under study, which were obtained by electrochemical insertion,[4,5,8,9] show that for all of them the insertion proceeds via phase

(27) McCusker, L. B.; Von Dreele, R. B.; Cox, D. E.; Louer, D.; Scardi, P. J. *Appl. Crystallogr.* **1999**, *32*, 36.
(28) Sears, V. F. *Neutron News* **1992**, *3*, 26.
(29) Roche, C.; Chevrel, R.; Jenny, A.; Pecheur, P.; Scherrer, H.; Scherrer, S. *Phys. Rev. B* **1999**, *60*, 16442.
(30) Mancour-Billah, A.; Chevrel, R. *J. Solid State Chem.* **2003**, *170*, 281.
(31) Levi, E.; Mitelman, A.; Aurbach, D.; Isnard O. *Inorg. Chem.* **2007**, *46*, 7528.
(32) Levi, E.; Mitelman, A.; Isnard, O.; Brunelli, M.; Aurbach, D. *Inorg. Chem.* **2008**, *47*, 1975.

transitions with the first stage, $Mo_6T_8 \rightarrow MMo_6T_8$, that is, it results in the formation of stoichiometric compounds ($x = 1$). (In the original work[4,5] it was suggested that the first intercalation compounds formed in the Na systems are $Na_3Mo_6T_8$, but we believe[21] that this was a misunderstanding). Thus, the cation occupancy in cavity 1 was kept fixed at 1/6, which corresponds to one cation per formula unit. The possibility of cation location in other sites was also checked in the refinement. For instance, as will be shown below, the potential energies of the inner and outer sites in $ZnMo_6S_8$ are close; thereby Zn dispersion between both of the sites seems to be probable. However, the fitting shows that the occupancy of the outer sites by Zn in the sulfide is negligible (0.004).

Hence, the refinement confirms that all seven compounds can be defined as classic CPs with different cation delocalization from the origin of cavity 1, which correlates well with the length R_i of the ideal chemical bond, M−T (Figure 3). The latter can be calculated according to the cation CN, its oxidation state V, and the tabulated bond-valence parameters for the "cation-anion" pairs R_0:[33,34]

$$R_i = R_0 - b \ln(V/CN) \quad (1)$$

Here b is the empirical constant equal to 0.37 Å, while the cation oxidation state V can be determined using the bond valence sum (BVS) equation:

$$V = \sum s_{ij} = \sum \exp[(R_0 - R_{ij})/b] \quad (2)$$

where R_{ij} is the distance (obtained in the refinement) between cation i and its neighbor anion j, and s_{ij} is the electrostatic bond strength.

The data of Table 2 were used to draw the maps of all the cation sites for the materials under study (Figures 4a−g). Here the circles represent the cation sites in the CP's crystal structure, while the numbers inside the circles are the BVS for these sites. The closer the BVS to the formal electrostatic charge of cation in ionic compounds, the more appropriate is its environment (anion polyhedron) for cation accommodation. The sites occupied by cations are marked in blue, while light and dark gray colors are used to distinguish (according to the BVS values) between empty sites suitable and problematic for cation intercalation, respectively. Thick circular lines mark the positions that are excessively close to the Mo atoms. The tables in the maps represent the shortest distances between the cation sites M_i and the Mo atoms.

Thus, the potential energy of any site can be roughly estimated according to the distances of these sites from adjacent anions and cations (by the BVS value and the shortest M_i−Mo distance, respectively). For proper analysis, the character of interactions between molybdenum and inserted cation should be taken into account. A comparison of Figure 4 panels a−g shows that each cation has its own map because of the adaptation of the Mo_6T_8 framework to cation size and character. As a result, the relative energy of cation sites differs for different compositions, and the sites, although inappropriate for insertion or transport of one cation, may be convenient for another one. More information about the maps for other CPs, as well as examples of their use, can be found in our previous papers.[21,24,32]

Dynamic Character of Cation Delocalization for "Big" Cations. Since the concept of blocked cations mentioned in the Introduction was used to explain the Na trapping in Mo_6T_8,[4,5] the details of the $NaMo_6T_8$ crystal structure appear to be crucial for understanding the mechanism of ionic transport in CPs.

In contrast to the Zn-, Cd-, and Mn-containing CPs, the refinement does not allow an unambiguous determination of the Na position in the $NaMo_6T_8$ crystal structure because the R-factors obtained for two different models (I, Na is in the tetrahedral sites, and II, Na is in the center of cavity 1 coordinated by two T_2 anions) are too close. It can be suggested that this uncertainty in the cation position results from the similar values of the potential energy for these two sites. According to the BVS values (0.89), the central site in $NaMo_6S_8$ is slightly too large for Na^+ cation accommodation; thereby, the cation shift from the origin of cavity 1, which should stabilize the structure, seems more probable. In any case, this shift should be quite small and close to that for Ag (0.26 Å for $AgMo_6S_8$[18]). For $NaMo_6Se_8$, the BVS value (0.96) of the central site (CN = 2) is more convenient for Na^+ than that of the tetrahedral site (1.36). Thus, in agreement with previous works,[4,5] $NaMo_6T_8$ should be related to type I of classic CPs.

As can be seen from Table 2, Na^+ ions located in the center of pseudo-cubic cavity 1 are coordinated only by two of eight anions because the BVS values for CN = 8 greatly exceed the formal cation charge. However, CN = 2 is in contradiction with the almost linear correlation between the cation position in cavity 1 and the length of the ideal chemical bond presented in Figure 3. Actually, according to the latter, the value of the cation delocalization in $NaMo_6T_8$ correlates well with CN equal to 4 and 8, but not with CN = 2. Similarly, for $AgMo_6S_8$ a small cation shift is consistent only with CN = 8. It seems that this apparent increase in the CN is not accidental but follows from the dynamic character of the cation delocalization in these compounds when the energy of the thermal vibration at RT is enough to overcome the activation energy of hopping between the tetrahedral sites of the inner ring. Such interpretation of the cation delocalization was proposed by Yvon for Cu^+ in $Cu_xMo_6S_8$ ($1.8 \leq x \leq 3.66$).[18]

The spontaneous circular motion for Ag^+ or Na^+ in MMo_6T_8 at RT seems to be even more probable than that for Cu^+ because of the smaller shift of these cations from the origin of cavity 1. Actually, the smaller the diameter of the inner ring, the shorter is the hopping length, M_1−M_1, and the lower the potential barrier of the cation motion between the M_1 sites (because of lower M−Mo repulsion, evidenced by the longer M_1−Mo distances). Moreover, the cation motion within the inner ring should be energetically favorable because it results in a uniform bonding between the cation and the six equivalent T_1 anions, as well as in a homogeneous distribution of the cation charge in cavity 1.

This local cation motion agrees well with our previous conclusion:[21] The immobility of "big" cations such as Na,

(33) Brese, N. E.; O'Keefee, M. *Acta Crystallogr.* **1991**, *B47*, 192.
(34) Brown, I. D. *Acta Crystallogr.* **1992**, *B48*, 553.

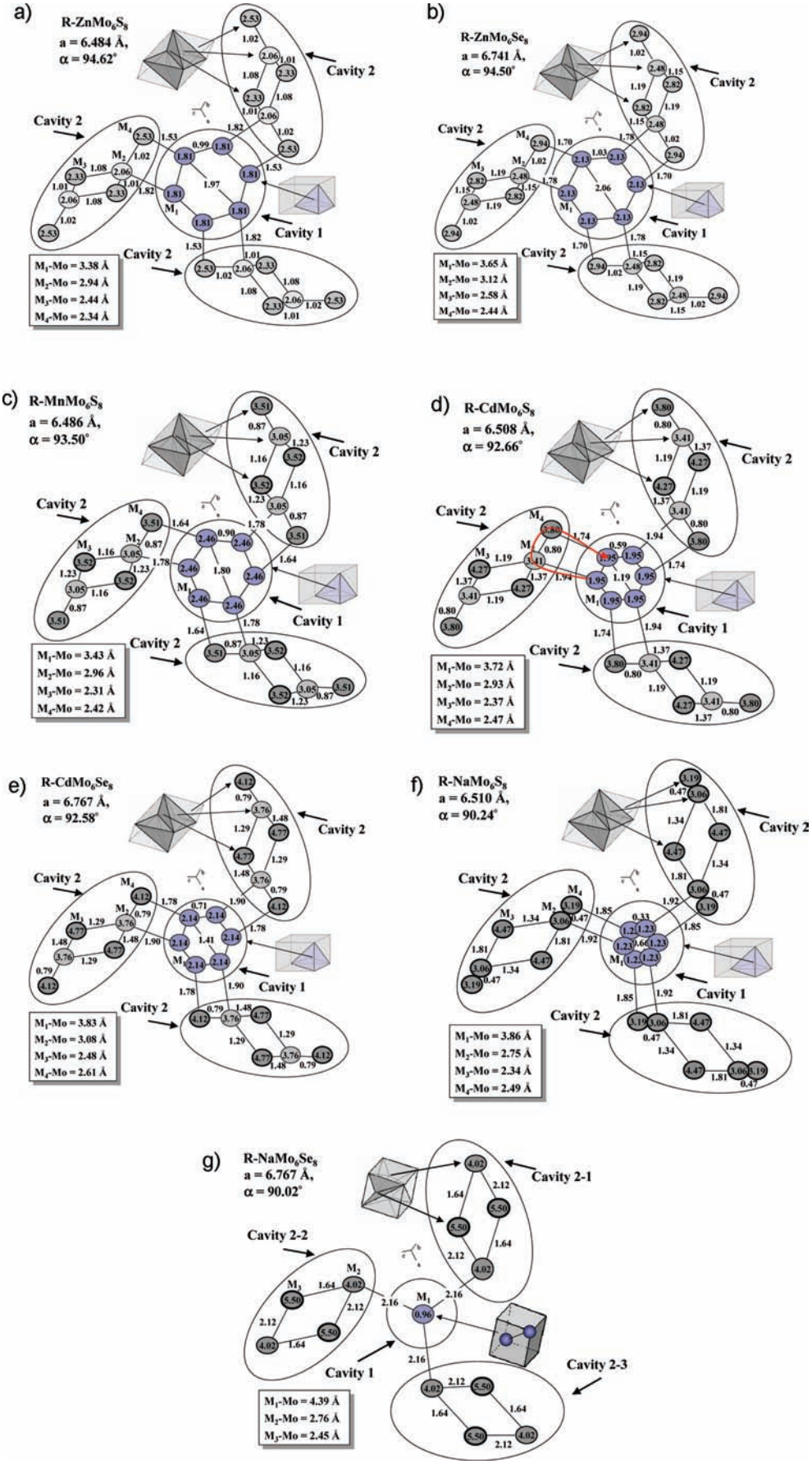

Figure 4. Maps of the cation sites for the materials under study: (a) $ZnMo_6S_8$, (b) $ZnMo_6Se_8$, (c) $MnMo_6S_8$, (d) $CdMo_6S_8$, (e) $CdMo_6Se_8$, (f) $NaMo_6S_8$, (g) $NaMo_6Se_8$. The projections are normal to −3 symmetry axis. The inserts show the polyhedral structure of cavities 1 and 2 (The orientation of the polyhedra is not related to the translation vectors). The occupied sites are in blue (Note that the occupation of the inner sites in Figures 4a−f is random).

Table 3. Structural Parameters of CPs under Study (Continuation) [a]

				cation position: site M_1					
N	CP	CN	ideal chemical bond, M−T, Å	*x*	*y*	*z*	occ.	BVS	delocalization, Å
1	$NaMo_6S_8$	8	3.05	0	0	0	1/6(fixed)	1.49	0
		4	2.79	0.688(5)	0.385(3)	0.332(3)	1/6(fixed)	1.23	0.33
		2	2.54	0	0	0	1/6(fixed)	0.86	0
2	$NaMo_6Se_8$	8	3.18	0	0	0	1/6(fixed)	1.81	0
		4	2.92	0.680(5)	0.366(3)	0.332(2)	1/6(fixed)	1.36	0.27
		2	2.67	0	0	0	1/6(fixed)	0.96	0
3	$CdMo_6S_8$	4	2.55	0.646(6)	0.262(2)	0.334(1)	1/6(fixed)	1.95	0.59
4	$CdMo_6Se_8$	4	2.66	0.633(6)	0.251(1)	0.335(2)	1/6(fixed)	2.14	0.70
5	$MnMo_6S_8$	4	2.37	0.617(3)	0.223(2)	0.329(3)	1/6(fixed)	2.46	0.90
6	$ZnMo_6S_8$	4	2.35	0.707(2)	0.451(1)	0.331(2)	1/6(fixed)	1.81	0.99
7	$ZnMo_6Se_8$	4	2.48	0.785(1)	0.373(3)	0.331(2)	1/6(fixed)	2.13	1.03

[a] BVS = bond valence sum; delocalization refers to the cation position M1.

Ag, Sn, and Pb in CPs is only apparent; they become mobile in the case where the pushing forces of additional inserted cations (related to their mutual repulsion) are high enough to overcome the E_d energetic barriers.

Variations in the Transport Behavior of "Small" Cations Caused by Subtle Changes in the Energetic Structure of Cavity 2. As can be seen in Figure 3, the delocalization of cations such as Zn^{2+}, Mg^{2+}, $Mn^{2.5+}$, and Li^+ is relatively similar in magnitude. Thus, it should be expected that these cations would have a similar diffusivity in CPs. However, this is not exactly the case: Zn and Li are highly mobile over the entire intercalation range (up to $x = 2$ and 4, respectively) for both sulfides and selenides,[5−7,11] while Mn and Mg present kinetic limitations in the sulfides, for $x < 1$.[8,21,22] This phenomenon can be partly explained by the different oxidation state of the inserted cations. In fact, the larger the cation charge, the stronger is its repulsion from the Mo atoms, and the higher are the energetic barriers for its diffusion. Therefore, the insertion of the monovalent Li^+ ion should be a priori faster than that of the divalent cations.

Similarly, Mn insertion should be a priori slower than that of divalent cations because its mean oxidation state in $MnMo_6T_8$ is equal to 2.5 (see the BVS value for $MnMo_6S_8$ in Table 3) [Interestingly, $MnMo_6S_8$ was obtained by high temperature synthesis, but the same material can be prepared by an electrochemical reaction in aqueous Mn^{2+} solutions.[8] The insertion proceeds via three stages, while the stoichiometry of the fully intercalated product, $Mn_2Mo_6S_8$, corresponds to a divalent Mn^{2+}. This means that Mn insertion results not only in the reduction of the Mo_6-cluster but also in uncommon changes in the oxidation state of the inserted cations at different intercalation stages. As a result, the phase diagram for the $Mn-Mo_6T_8$ systems[8] is not similar to that of other divalent cations, but more complicated]. However, we have to take into account that the diffusivity of Mn as a transition metal may be higher because of possible metallic interactions with Mo in the M_3-transport sites.[21,29] Thus, it is difficult to explain the difference in the diffusion kinetics in the CPs only by the cation charge effect. To clarify this point, let us look more thoroughly at the structural changes in cavity 2, which take place with the insertion of different cations. In a previous work,[21] we estimated the potential energies of the cation sites, M_1, M_2, and M_3, related to the two competing diffusion pathways, M_1-M_1 and $M_1-M_2-M_3-M_2'-M_1'$

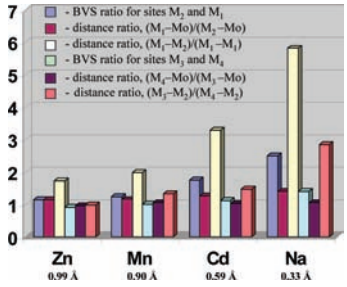

Figure 5. Structural parameters of the sulfides under study affecting cation mobility. X-axis presents the inserted cation and its delocalization.

(Figure 2). We emphasized the crucial role of the M_3-sites as a bottleneck for the progressive diffusion, whereas the peripheral M_4 sites in cavity 2 were, a priori, excluded from consideration because of their commonly short distance from the Mo atoms. In addition, we focused on changes in cavity 1 caused by the insertion of different cations, while the structure of cavity 2 was accepted as being relatively invariable.

A more careful analysis of the presented maps (Figures 4a−g) shows that the energetic structure of cavity 2 in MMo_6T_8 compounds is not constant, but changes with increasing the cation size, mainly by shortening the M_2-M_4 distance. (Note that finally the two tetrahedral sites in the compounds with "small" cations join to form a single square-pyramid in the case of "big" cations). The closer approach of the M_2 and M_4 sites is associated with the increase in the M_4-Mo distance, as well as with a larger M_4 interstitial, evidenced by the smaller BVS values. As a result, the potential energy, E_4, should be comparable with E_3, and even lower, while the M_2-M_4 distance becomes effectively smaller than the M_2-M_3 separation. In such a case, the cation, which begins its progressive diffusion by jumping from the inner to the outer site, may prefer to return to the same inner ring through the M_4 site, instead of hopping to the M_3 site. The additional pathways, $M_1-M_2-M_4-M_1$, with the circular cation motion, clearly seen in the $CdMo_6T_8$ and $NaMo_6T_8$ maps (see the red line in Figure 4d), should hamper the ionic transport in the bulk and increase the possibility for cation trapping at $x < 1$.

Figure 5 illustrates the variations in the geometry of the crystal structure for the sulfides under study. For simplicity, we do not use all the structural parameters affecting the E_d/E_c ratio,[21] but only three of them: the BVS ratio for

sites M_2 and M_1 and two distance ratios, $(M_1-Mo)/(M_2-Mo)$ and $(M_1-M_2)/(M_1-M_1)$. As can be seen, the lower the cation delocalization, the larger are the chosen parameters, that is, the higher is the chance for a circular motion within the inner ring and the slower is the progressive diffusion. This change is accompanied by bigger values for the other three parameters, namely, the BVS ratio for sites M_3 and M_4, and two distance ratios, $(M_4-Mo)/(M_3-Mo)$ and $(M_3-M_2)/(M_3-M_4)$, which, in turn, are responsible for the higher probability of the cation returning from the outer to the inner site through additional pathways, as discussed above. As a result of these consistent changes, a relatively small decrease in cation delocalization may be crucial for cation mobility (e.g., when Mn replaces Zn in MMo_6S_8).

Conclusions

A combined Rietveld analysis of powder X-ray and high-resolution neutron diffraction profiles was used to determine the exact cation locations in the crystal structures of $NaMo_6T_8$, $ZnMo_6T_8$, $CdMo_6T_8$, and $MnMo_6S_8$. All seven compounds can be defined as classic CPs, where cation delocalization from the center of the largest cavity between the Mo_6T_8 blocks decreases with the length of the ideal chemical bond, M−T. Minimal delocalization (between zero and 0.33 Å) was found for $NaMo_6T_8$, which, in agreement with previous work[4,5] can be classified as type I of classic CPs.

Our analysis shows that Na^+ ions in $NaMo_6T_8$ are not completely immobile; they do not block the ionic transport, as was suggested previously.[3−5] The small delocalization of "big" cations, such as Na^+ and Ag^+, has a rather dynamic character, that is, the energy of the thermal vibration at RT is enough to overcome the activation energy of hopping between the tetrahedral sites of the inner ring, E_c. Thus, this work confirms our previous conclusion:[21] The immobility of "big" cations, like Na, Ag, Sn, and Pb in CPs, is only apparent; they become mobile in cases where the pushing forces of additionally inserted cations (related to their mutual repulsion) are high enough to overcome the energetic barriers of progressive diffusion, E_d, for example, in $Na_xMo_6T_8$ for $x > 1$.

In contrast to a previous study,[21] this work does not limit the diffusion analysis to two competing pathways of inserted ions (circular motion within the same cavity between the Mo_6T_8 blocks and progressive diffusion from one cavity to adjacent one) but takes into account an additional circular pathway through the transport sites in both cavities 1 and 2 (inner, outer, and peripheral sites). Cation motion along this pathway decreases the chance of progressive diffusion. The improved diffusion analysis explains the exceptional sensitivity of the ionic mobility in CPs to peculiarities of their crystal structure.

Acknowledgment. Partial support for this work was obtained from the Israel−U.S. Binational Foundation (BSF). The Institut Laue Langevin is warmly acknowledged for providing the neutron facilities. We wish to express our deep gratitude to Prof. A. Belostotsky, Dr. Y. Gofer, and Dr. G. Salitra for their assistance with the synthesis.

Supporting Information Available: Crystallographic information in the form of cif files. The Rietveld profiles for the materials under study. Additional data related to mobility of Na, Cd, Mn and Zn in CPs. This material is available free of charge via the Internet at http://pubs.acs.org.